FIRST–a fibered aperture masking instrument: on-sky results

Elsa Huby[a], Guy Perrin[a], Franck Marchis[b], Sylvestre Lacour[a], Takayuki Kotani[c], Gaspard Duchêne[d,e], Elodie Choquet[a], Elinor Gates[f], Julien Woillez[g] and Olivier Lai[h]

[a]LESIA, Observatoire de Paris, CNRS, UPMC, Université Paris-Diderot, Paris Sciences et Lettres, 5 place Jules Janssen, 92195 Meudon, France ;
[b]Carl Sagan Center at the SETI Institute, 189 Bernardo Av., Mountain View CA 94043, USA ;
[c]ISAS/JAXA, 3-1-1 Yoshinodai, Chuo-ku, Sagamihara 252-5210 Japan [d]Department of Astronomy, University of California at Berkeley, Hearst Field Annex, B-20, Berkeley CA 94720-3411, USA ;
[e] UJF-Grenoble 1 / CNRS-INSU, Institut de Planétologie et d'Astrophysique de Grenoble (IPAG) UMR 5274, Grenoble, F-38041, France
[f]University of California Observatories/Lick Observatory, P.O. Box 85, Mount Hamilton, CA 95140, USA ;
[g]W. M. Keck Observatory, 65-1120 Mamalahoa Hwy, Kamuela, HI 96743, USA ;
[h]Canada-France-Hawaii Telescope, 65-1238 Mamalahoa Hwy, 96743 Kamuela, HI, USA.

ABSTRACT

We present on-sky results obtained with the visible light prototype of the Fibered Imager foR Single Telescope (FIRST) mounted on the 3-m Shane Telescope at Lick Observatory and using its Adaptive Optics system. This instrument is dedicated to high angular resolution and high dynamic range imaging. Its principle combines both techniques of single-mode fiber interferometry and pupil remapping. Simulations predict a dynamic range up to 10^6 at λ/D, or at a few tens of milliarcseconds at 630 nm using an 8-m telescope. Laboratory experiments based on a 9-fiber prototype working in the 600 nm–900 nm spectral band successfully demonstrated the power of the concept. The same prototype has been set-up on the 3-m Shane telescope in July 2010. In this paper, we present the on-sky results obtained in October 2011 with an improved version of the instrument using 18 fibers. They clearly show the detection of the binary star Capella at the diffraction limit of the telescope.

Keywords: high dynamic range imaging, high angular resolution, aperture masking, pupil remapping, fiber interferometer, Capella, exoplanets

1. INTRODUCTION

The search and characterization of faint objects such as exoplanets is nowadays one of the most challenging domains in instrumentation. Indeed, the detection of companions orbiting around a parent star requires high performances in angular resolution and dynamic range, since the separation between them is very small and the flux ratio is high. Depending on the wavelength of observation and on the distance of the planet, this ratio can be as low as 10^{-3}–10^{-5} for hot Jupiters down to 10^{-8} in the visible.[1] The difficulty is increased for closer planets, hence the necessity to reach and beat the diffraction limit λ/D. Reaching such high performances is particularly challenging for ground-based instruments that are subject to turbulent atmosphere.

Different techniques have been developed in order to overcome this limitation. Adaptive Optics (AO) for instance, offers a way to retrieve the diffraction limit of a telescope. Its principle is based on an active correction of the incident wavefront thanks to a deformable mirror. Important planet discoveries by direct imaging have been made possible by the use of AO on large telescopes, such as the planets around HR 8799[2,3] and around β Pictoris.[4] Both detections were achieved for planet-to-star flux ratio of 10^{-4} to 5×10^{-5} (in K_s and L' bands) at separations of a few λ/D. However, wavefront correction cannot be perfect and residual speckle noise is still the cause for dynamic range limitation.

Post-processing techniques that take advantage of very short exposure images to freeze turbulence, such as speckle interferometry,[5] are also efficient to reach the diffraction limit, but speckle noise limits dynamic range to a few 100. The aperture masking[6] technique using a non-redundant pupil mask is now a standard for high resolution imaging with contrast ratios on the order of 10^{-3} at λ/D.[7,8] However, the drawback of this method is that the non-redundancy of the mask necessitates that the fraction of the pupil that collects light is small (a few percent of the whole pupil). In addition, speckle noise may remain across the sub-pupils. The Keck segment-tilting experiment[9] is a trick to use aperture masking with the whole pupil but the limitation due to speckle noise still remains.

In order to bypass these limitations, the concept of pupil remapping combines the aperture masking technique with the use of single-mode fibers.[10] This allows to almost completely remove the speckle noise and to use the whole pupil. Simulations on the performances of this technique have shown that dynamic ranges on the order of 10^{-6} could be reached on an 8-m telescope at visible wavelengths, using 132 sub-pupils, and assuming pure photon noise limitation, 40 s exposure time and 0.5 arcsec seeing.[11] A prototype of this instrument called FIRST (Fibered Imager foR a Single Telescope) was developed and tested at Paris Observatory. It works in the 600 nm–900 nm spectral band and used at first 9 fibers out of the 30 available fibers. The results have shown that image can be recovered from visibility and phase measurements. A new version of the instrument, called FIRST-18 because it uses 18 fibers, was then tested at Lick Observatory. The prototype is mounted on the 3-m Shane telescope, behind the AO system. In this paper we present the results on stellar targets.

2. THE 18-FIBER PROTOTYPE

The current prototype, has been built from the FIRST-9[12] version of the instrument. The injection part is identical: a segmented mirror (*Iris AO*) is used to precisely steer beams and maximize the injection efficiency into the fibers. Microlenses focus the light on the fiber cores that are gathered in a fiber bundle. The recombination part has been doubled, as can be seen on Fig. 2. Indeed, 18 fibers out of the 30 available fibers are now used. They are bundled into two sets of 9 fibers, each set being recombined independently from the other set. Both configurations of the sub-pupils in the entrance pupil can be seen on Fig. 2. Combination of both fiber sets gives access to around 70% of the total (u,v) coverage that should be available with a full pupil, and to 168 closure phase measurements.

As for the 9-fiber version, beams are spectrally dispersed thanks to an equilateral SF2-prism. The spectral resolution is increased by stretching the beams along the dispersion direction and compressing them in the orthogonal direction, thanks to an afocal anamorphic system consisting of cylindrical lenses.

The injection optimization procedure has also been improved by dedicating one part of the set-up to image the v-groove ends. This allows to monitor the transmitted flux in each fiber on one camera, and to simultaneously maximize the injection efficiency by steering the corresponding segments. The procedure is automated and takes only 3–5 minutes to optimize the tilts of the 18 segments. Every time we switch between targets, motorized mirrors allow for rapid toggling between the acquisition and optimization modes.

3. DATA REDUCTION

A data sample is shown in Fig. 3. Two interference patterns can be seen on the left and right in the image, corresponding to the recombination of the two sets of 9 fibers. Spectral filters have been put in each arm to avoid overlapping of the patterns in the central part of the camera. Both patterns are reduced separately.

At the anamorphic system output, the Gaussian beams have particularly small waist along the direction orthogonal to the dispersion direction (around 40 μm). As a consequence, they are rapidly diverging when passing through the 2-inch prism. This induces a strong astigmatism aberration in the diffraction pattern of a single fiber, resulting in a "banana-shaped" line instead of a vertical straight line, as can be seen for the monochromatic beam in the right part of Fig. 3.

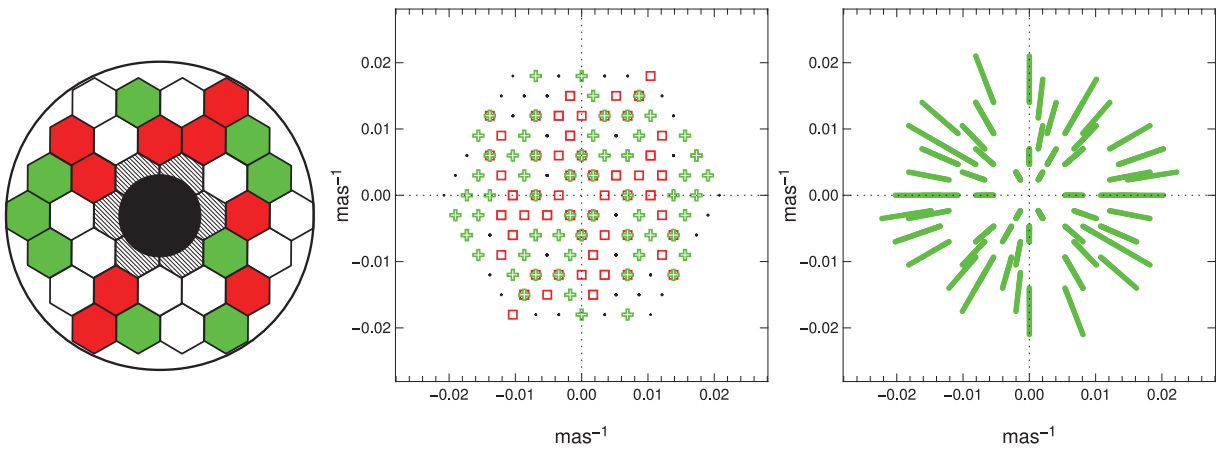

Figure 1. *Left:* Entrance pupil configurations with the two sets of 9 sub-pupils. *Middle:* Total (u,v) plane coverage at 700 nm, that represents around 70% of all available spatial frequencies. The green and red symbols correspond respectively to the green and red configurations. *Right:* (u,v) plane coverage corresponding to the green configuration including the wide spectral band, from 600 nm to 900 nm.

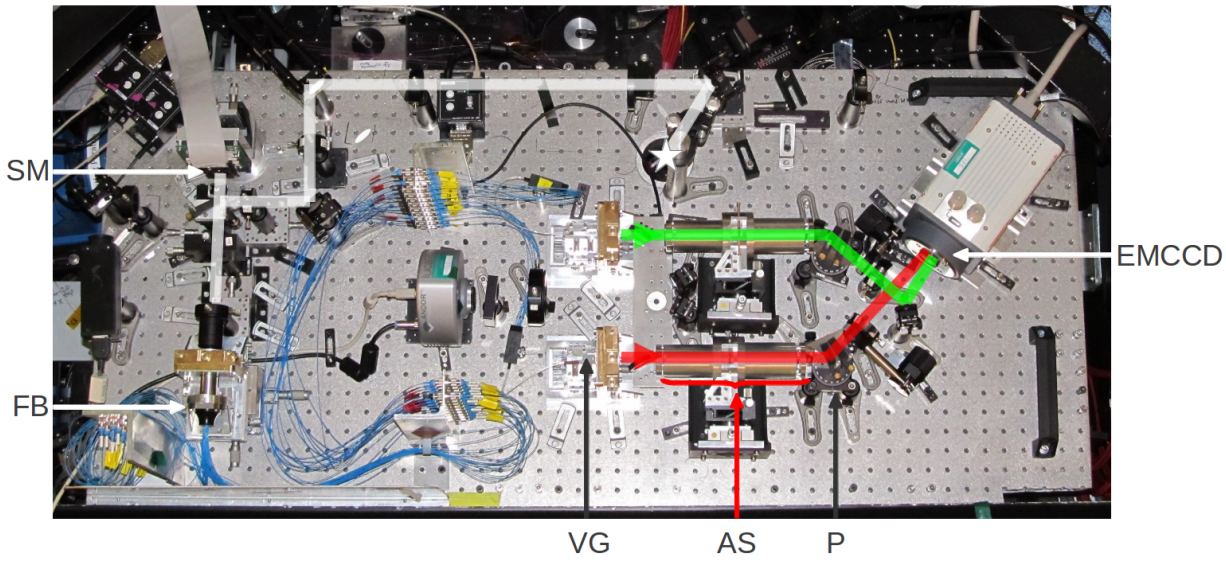

Figure 2. Picture of the FIRST-18 bench. The white star represents the beam entrance on the bench (coming from below). The beam path is drawn in *white* for the injection part of the set-up. This part includes the segmented mirror (*SM*) and the fiber bundle (*FB*). The beams in the recombination parts are drawn in *red* and *green* to distinguish both sets of fibers. The positions of the v-groove (*VG*), anamorphic system (*AS*) and prism (*P*) are shown for one path but are symmetrically positioned for the other one.

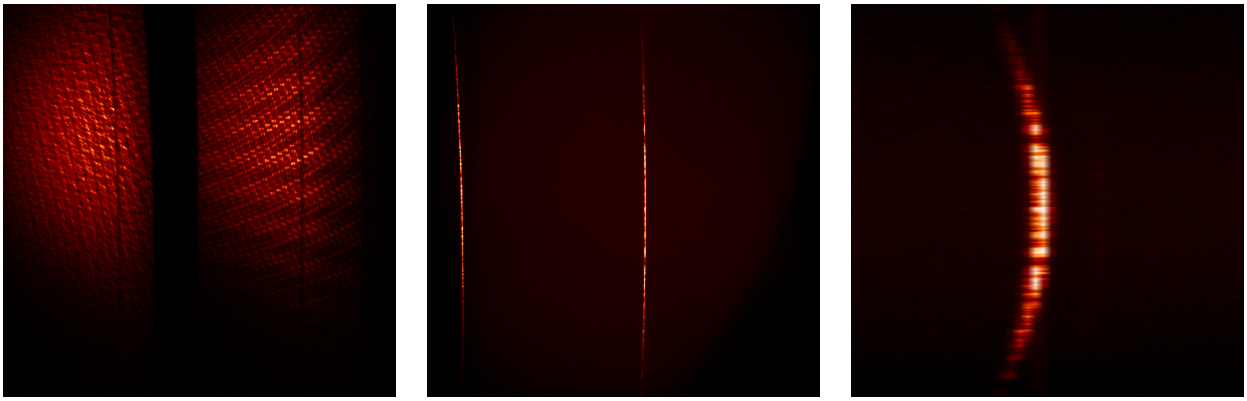

Figure 3. *Left:* Typical image acquired on the EMCCD camera where the two interference patterns can be seen. This image has been taken on Capella (R_{mag}=0.4) with 50 ms integration time, EM gain set to 1200 and under good seeing conditions (r_0 on the order of 15 cm). The optical path difference varies along the vertical direction, while the wavelength varies along the horizontal direction, increasing from left to right for both patterns. *Middle:* Fringes acquired on the laser source (633 nm) provided by the AO system. *Right:* Zoom-in on one monochromatic diffraction pattern where the distortion due to optical aberration clearly appears.

The data reduction steps are described below:

- correction of the distortion in the diffraction pattern by spline interpolation ;
- dark subtraction ;
- wavelength calibration by fitting the stellar spectrum ;
- fringe fitting in the image plane using the P2VM method[13] on every column ;
- bispectrum computation as a function of wavelength and closure phase computation.

4. RESULTS

Results have been obtained on the binary star Capella (G0III and G8III, R_{mag}=0.4). The predicted separation between the two components was 55 mas at the date of the observations and the flux ratio is around 1 in the visible.[14] Although the flux ratio is not high, this target is interesting for testing the performances of FIRST, as the separation is close to the diffraction limit of the telescope, which is 48 mas for a 3-m telescope at 700 nm. Aldebaran (K5III star, R_{mag}=0.1) has been chosen as calibrator since it is not resolved by the telescope.

Raw closure phase measurements as a function of wavelength for two different baseline triangles are shown in Fig. 4. 1000 images acquired on target and calibrator have been used to produce these results. Integration time was set to 50 ms per image and the EM gain was set to the maximum value of 1200. The 1000 images have been gathered into sets of 50 images leading to 20 measurements for each spectral channel and each baseline triangle. The error bars that are drawn in Fig. 4 are the statistical dispersion from the 20-measurement population. The average values of the error bars over the spectral bands are shown in Table 1.

The closure phase noted A corresponds to a relatively small triangle in the entrance pupil and as a consequence, no signature of the binary is detected. That means that the binary is not resolved by either of the spatial frequencies that form the triangle, leading to an average calibrated closure phase of $-0.3 \pm 0.1°$, as shown in Fig. 4. This non-zero value actually results from uncalibrated bias. This bias can be as high as a few degrees in the worst cases and results from systematic errors that do not average over long acquisitions. They may be the limiting factor for dynamic range performances, as it is the case in aperture masking measurements.[8] However their source still remains to be understood.

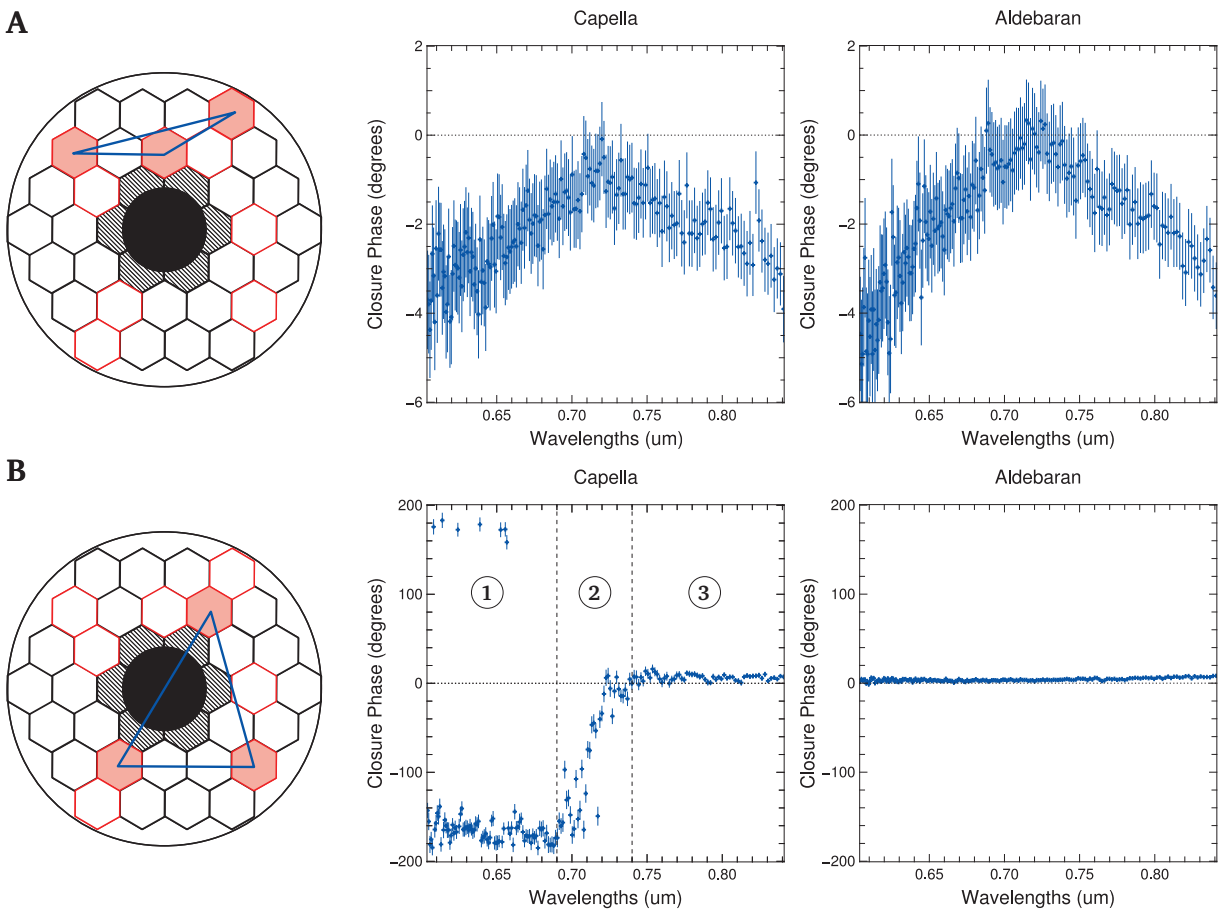

Figure 4. Raw closure phase measurements for two different triangles noted **A** and **B**. The closure phases are in degrees and are shown as a function of wavelength. *Left:* The corresponding baseline triangles represented in the entrance pupil. *Middle:* Closure phase measurements obtained on Capella for both triangle baselines. For triangle *B*, three spectral regions have been labelled **1** (before transiting region), **2** (transiting region) and **3** (after transiting region). *Right:* Closure phase measurements obtained on Aldebaran (calibrator) for both triangle baselines.

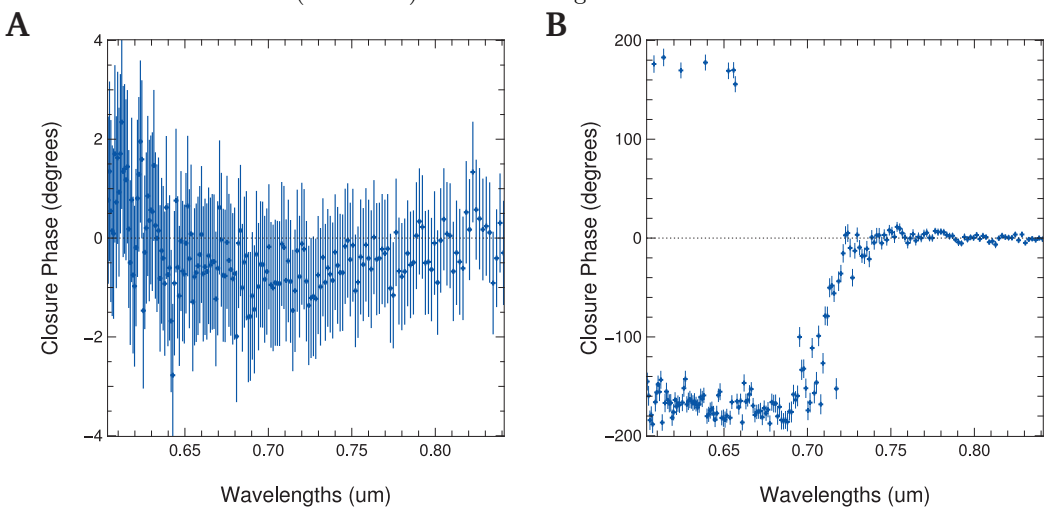

Figure 5. Calibrated closure phase measurements for Capella as a function of wavelength, obtained for baselines **A** and **B**, respectively on the left and on the right.

Table 1. Mean error bars obtained for raw closure phases **A** and **B**.

	CP A	CP B		
Capella	0.9 °	band 1 7.7°	band 2 9.0 °	band 3 3.6 °
Aldebaran	1.0 °	1.4 °		

On the other hand, the baseline triangle for closure phase B is built from higher spatial frequency vectors. It is clear that a strong signal appears in the closure phase of Capella, that cannot be seen for Aldebaran. The phase shifts from -180° to 0°, which is typical of a symmetric binary. Error bars are higher for Capella in this case as a phase shift occurs when the visibility goes through 0.

5. CONCLUSION

The preliminary results presented in this paper are promising as they clearly show that the binary star Capella is resolved albeit just at the diffraction limit of the telescope. Next steps of the data reduction will include fitting of the 168 spectral closure phase measurements to a binary model to retrieve the separation and the flux ratio at the time of the observation. The statistical error bars on the closure phase measurements are in the best case on the order of 1° per spectral channel. If accuracy was limited by these statistical errors (assuming that biases are corrected), dynamic ranges of a few 100 could be achieved with the FIRST-18 instrument. This prospective performances will be improved in the future by increasing the number of sub-pupils and the accuracy on the closure phase measurements (longer integration times) and by a better understanding of the bias sources.

ACKNOWLEDGMENTS

The authors would like to thank Dr. Bolte, Director of the University of California Observatories for his commitment and financial support, as well as the Lick Observatory staff for its precious help during every runs. We acknowledge financial support from Programme National de Physique Stellaire (PNPS) of CNRS/INSU, France and Observatoire de Paris.

REFERENCES

[1] Demory, B.-O. and Seager, S., "Hot jupiter secondary eclipses measured by kepler," *EPJ Web of Conferences* **11**, 03005 (2011).

[2] Marois, C., Macintosh, B., Barman, T., Zuckerman, B., Song, I., Patience, J., and Lafrenière, "Direct imaging of multiple planets orbiting the star hr 8799," *Science* **322 no. 5906**, 1348–1352 (2008).

[3] Marois, C., Zuckerman, B., Quinn, M. K., Macintosh, B., and Barman, T., "Images of a fourth planet orbiting hr 8799," *Nature* **468**, 1080–1083 (2010).

[4] Lagrange, A.-M., Bonnefoy, M., Chauvin, G., Apai, D., Ehrenreich, D., Boccaletti, A., Gratadour, D., Rouan, D., Mouillet, D., Lacour, S., and Kasper, M., "A giant planet imaged in the disk of the young star β pictoris," *Science* **327 no. 5987**, 57–59 (2010).

[5] Labeyrie, A., "Attainment of diffraction limited resolution in large telescopes by fourier analysing speckle patterns in star images," *A&A* **6**, 85 (1970).

[6] Haniff, C. A., Mackay, C. D., Titterington, D. J., Sivia, D., Baldwin, J. E., and Warner, P. J., "The first images from optical aperture synthesis," *Nature* **328**, 694–696 (1987).

[7] Hinkley, S., Carpenter, J. M., Ireland, M., and Kraus, A. L., "Non-redundant aperture masking constraints on massive companions within 12 au of the hr 8799 system," *The Astrophysical Journal* **730**, L21 (2011).

[8] Lacour, S., Tuthill, P., Amico, P., Ireland, M., Ehrenreich, D., Huelamo, N., and Lagrange, A.-M., "Sparse aperture masking at the vlt," *A&A* **532** (2011).

[9] Monnier, J. D., Tuthill, P. G., Ireland, M., Cohen, R., Tannirkulam, A., and Perrin, M. D., "Mid-infrared size survey of young stellar objects: description of keck segment-tilting experiment and basic results," *The Astrophysical Journal* **700**, 491–505 (2009).

[10] Perrin, G., Lacour, S., Woillez, J., and Thiébaut, E., "High dynamic range imaging by pupil single-mode filtering and remapping," *MNRAS* **373**, 747–751 (2006).

[11] Lacour, S., Thiébaut, E., and Perrin, G., "High dynamic range imaging with a single mode pupil remapping system : a self calibration algorithm for redundant interferometric arrays," *MNRAS* **374**, 832–846 (2007).

[12] Huby, E., Perrin, G., Marchis, F., Lacour, S. andKotani, T., Duchêne, G., Choquet, E., Gates, E. L., Woillez, J. M., Lai, O., Fédou, P., Collin, C., Chapron, F., Arslanyan, V., and Burns, K. J., "First, a fibered aperture masking instrument. i. first on-sky test results," *A&A* **541**, A55 (May 2012).

[13] Millour, F., Tatulli, E., Chelli, A., Duvert, G., Zins, G., Acke, B., and Malbet, F., "Data reduction for the amber instrument," *Proc. SPIE* (2004).

[14] Torres, G., Claret, A., and Young, P. A., "Binary orbit, physical properties, and evolutionary state of capella (α aurigae)," *Astrophysical Journal* **700**, 1349–1381 (Aug. 2009).